



Highly selective recovery of Au(III) from wastewater by thioctic acid modified Zr-MOF: Experiment and DFT calculation

Chen Wang^{a,b,1}, Guo Lin^{d,1}, Jiling Zhao^{a,b}, Shixing Wang^{a,b,*}, Libo Zhang^{a,b,*}, Yunhao Xi^{a,b}, Xiteng Li^{a,b}, Ying Ying^c

^a State Key Laboratory of Complex Nonferrous Metal Resources Clean Utilization, Kunming University of Science and Technology, Kunming, Yunnan 650093, PR China

^b Faculty of Metallurgical and Energy Engineering, Kunming University of Science and Technology, Kunming, Yunnan 650093, PR China

^c Faculty of Science, Kunming University of Science and Technology, Kunming 650500, PR China

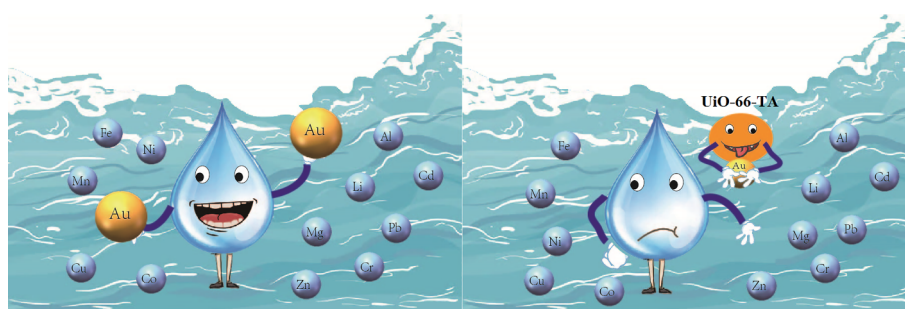
^d School of Materials and Metallurgy, Wuhan University of Science and Technology, Wuhan, Hubei 430081, PR China



HIGHLIGHTS

- The novel adsorbent was synthesized by functionalizing Zr-MOF with thioctic acid.
- The Au(III) capture capacity reached to 374 mg/g at pH 2.
- Adsorbent shows good reusability and selectivity for Au(III).
- DFT and XPS shows the adsorption mechanism is chelation and ion exchange.

GRAPHICAL ABSTRACT



ARTICLE INFO

Keywords:

Au
Wastewater
Adsorption
DFT
Mechanism

ABSTRACT

A novel adsorbent (UiO-66-TA) was presented by modifying metal-organic framework composites with thioctic acid. UiO-66-TA were characterized by fourier transform infrared (FT-IR), field emission scanning electron microscopy (FESEM), thermogravimetric (TG), Brunner-Emment-Teller (BET) measurement and X-ray photoelectron spectroscopy (XPS), which indicating that it had excellent morphology and specific surface area. The adsorption performances of UiO-66-TA for Au(III) were studied. The results showed that UiO-66-TA had a strong adsorption capacity under acidic conditions and the optimal pH was 2.0. Isotherm and kinetic adsorption were also conducted and found that the experimental values correspond to Langmuir model and pseudo-second-order isotherm model, indicating that the mechanism is mainly chemical adsorption on a uniform surface. Wastewater experiment showed that UiO-66-TA can be used for highly selective recovery Au(III) in actual life. The regeneration and thermodynamic experiments indicated that UiO-66-TA can be reused and were a spontaneous endothermic process. XPS analysis and the zeta potential proved that the main adsorption mechanisms were ion exchange and chelation. DFT calculation found that there are two ways to combine Au with S on UiO-66-TA and their distances are 2.38 Å and 2.39 Å, indicating that the gold and sulfur play a major role in chelation. In summary, UiO-66-TA was a hopeful adsorbent and could be used to collect gold ions from wastewater in a sustainability perspective.

* Corresponding authors at: Faculty of Metallurgical and Energy Engineering, Kunming University of Science and Technology, Kunming 650093, PR China.
E-mail address: wsxkm@126.com (S. Wang).

¹ These authors contributed equally to the paper.

1. Introduction

As a precious metal, gold has been popular in the jewelry and currency industries since ancient times. With the development of society, gold is widely used in electronic and electrical equipment and medical industry as an indispensable material [1]. Therefore, the output of gold is far behind the demand. Due to the gold is a scarce resource, the recovery of gold in various wastes has attracted widespread attention, including mine tailings, industrial waste electronic waste and leaching residue [2]. Generally, the gold is dissolved into acid solution through reacting with chlorine gas and formed anionic metal species [3]. Therefore, it is important to recover gold ions from aqueous solution.

In order to efficiently recycle gold ions from wastewater, various techniques have been developed, including solvent extraction, chemical precipitation, membrane separation, ion exchange, flotation and adsorption [4–7]. However, some of the above methods have disadvantages including low recovery, low economy, long recovery cycle, secondary pollution and etc. Recently, adsorption has received great attention and are widely used in practical applications attribute to the simple operation and low cost [8,9]. Nevertheless, the traditional adsorbents commonly presented some shortcomings such as low-capacity, poor selectivity and weak regenerative performance [10]. Hence, to overcome the above difficulties, it is urgently to produce a new-style adsorbent with excellent adsorption performance, remarkable repeatability and selectivity to separate Au(III) from wastewater.

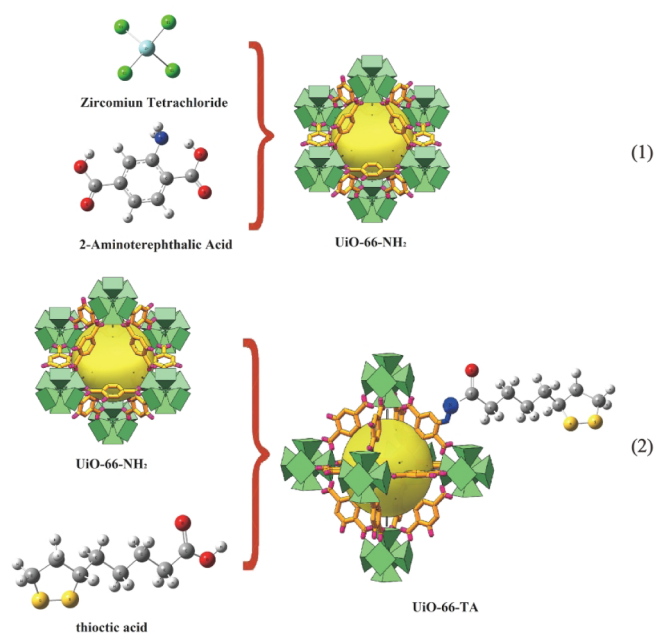
Metal-organic frameworks (MOFs) are a unique class of crystalline materials composed of organic ligands and metal ions/clusters by esterification reaction to form one/two/three dimensional structures [11]. Due to MOFs have the extraordinary performance including enormous specific surface areas, controllable pore size, flexible tailorability and ultrahigh porosity, it has been widely used in gas storage and separation, catalysis industry, sensors and biomedicine [12]. In addition, MOFs have also been applied to selective adsorb and separate the metal ions from aqueous solution. However, the structures of MOFs are vulnerable to damage and instability in water [13]. Herein, it is important to develop the MOFs with water stability and chemically resistant for selective adsorption metal ions from wastewater.

Some scholars have found that compared with Cu-based MOFs and Cr-based MOFs, Zr-based MOFs presented significant chemical, thermal stability and mechanical performance due to the strong Zr–O bonds [3]. UiO-66-NH₂ is a typical zirconium based MOF and has been widely used as adsorbent in aqueous solutions, such as lead, cadmium, copper, dye, fluoride, arsenate and dihydrogen arsenate [14–19]. The literatures prove that UiO-66-NH₂ is an effective adsorbent but lacks selectivity. In general, the most effective method is to modify UiO-66-NH₂ to give the excellent selectivity and maintain good adsorption capacity. UiO-66-NH₂ modified with 2,5-Dimercapto-1,3,4-thiadiazole remove selectively Hg(II) in water [20]. Ding et al found that the selective coefficient of thiol-modified Zr-MOFs for Hg(II) was as high as 28899.6 [13]. Therefore, post-synthetic modification has becoming an efficient and flexible strategy to improve selectivity. According to the hard soft acid-base (HSAB) principle, the thiol-containing groups have great affinity toward Au(III) [21]. In this work, thioctic acid modified Zr-MOF (UiO-66-TA) was prepared and used as selective adsorbent to recycle the Au(III) from wastewater. The impacts of initial pH, adsorption time, initial ions concentration and adsorption temperature during adsorption were investigated in detail. In addition, the binding energies between Au(III) and MOFs were calculated by density functional theory (DFT) to further obtain the adsorption mechanism.

2. Experimental and methods

2.1. Materials

Zirconium tetrachloride (ZrCl₄) was purchased from Tianjin



Scheme 1. Synthesis of UiO-66-NH₂ and UiO-66-TA.

Zhiyuan Chemical Reagent Co., Ltd. Thioctic acid, 2-aminoterephthalic acid, 1-(3-dimethylaminopropyl)-3-ethyl(EDC), N-hydroxysuccinimide (NHS), ethanol, dimethylformamide (DMF) were supplied by Aladdin Chemistry Co. Ltd. Gold solution, hydrochloric acid and sodium hydroxide were supplied by Shanghai Macklin Biochemical Co. Ltd. The above chemical reagents were of analytical grade and were not further purified. Distilled water is made by the laboratory. Wastewater comes from the laboratory.

2.2. Synthesized of UiO-66-types

UiO-66-NH₂ was synthesized through the published literatures [20]. After that, 0.01 mol EDC, 0.01 mol NHS, and 0.01 mol thioctic acid were sequentially added into 100 mL DMF. The mixture solution was stirred and reacted for three hours. Then, the solid and liquid were separated. Subsequently, 2.5 g UiO-66-NH₂ was added into the supernatant and stirred at 75 °C for 20 h. Finally, the precipitate was washed for five times with DMF and distilled water respectively. The product was obtained after drying for 12 h and named UiO-66-TA. The preparation methods of UiO-66-TA was illuminated in Scheme 1.

2.3. Characterization

Fourier transform infrared (FT-IR) spectroscopy was measured by Nicolet iS10 (Thermo, America). The thermogravimetric analysis (TGA) was measured by thermal Gravimetric Analyzer (PerkinElmer TGA-7 America) and at a heating speed of 10 °C/s until 800 °C. The morphology of UiO-66-TA was observed by field emission scanning electron microscopy (FESEM, JSM-7100F, JEOL) and transmission electron microscope (TEM, JEM-2100F, Japan). Pore structures and specific surface area of adsorbent were tested by Quantachrome Autosorb-1-C under –195.15 °C. Zeta potential was carried out using a NanoBrook-Omni (Brookhaven Instruments Co., USA) under pH 2.0–10.0. X-ray photoelectron spectroscopy (XPS) was conducted via a PHI-5000 Versaprobe II (Ulvac-Phi, Japan). The concentrations of Au(III) and impurity ions were analyzed using inductively coupled plasma atomic emission spectrometry (ICP-AES, Leeman Prodigy 7, America).

2.4. Adsorption experiments

Various experiments were conducted to investigate the adsorption capacity under different conditions, including pH, adsorption time and initial concentration of solution. In these experiments, 10 mg UiO-66-TA was put into 20 mL gold solution and shaken in a vibrator with 250 rpm at room temperature.

The relationship between pH and Au(III) removal rate was executed in a tube containing Au(III) and UiO-66-TA under pH 1.0–10.0. The initial concentration of Au(III) was 100 ppm (mg/L) and adsorption time was 20 h. After centrifugation, the residual content was detected by ICP-AES.

The adsorption isotherm tests were conducted with initial Au(III) concentration 150 ppm to 900 ppm, pH 2.0 and adsorption time 20 h. Adsorption kinetics experiments were carried out as follows: UiO-66-NH₂ and UiO-66-TA were added into 100 ppm of Au(III) solution and shaken for 10–480 min at pH 2.0, respectively.

The application of adsorbent to actual wastewater was carried out as follows: first, the pH of wastewater was adjusted to 2.0 to obtain the optimal pH value before the experiment. Then, the concentration of each metal ion in the wastewater was measured by ICP-AES. After that, 10 mg UiO-66-NH₂ and 10 mg UiO-66-TA were mixed with 20 mL wastewater and shaken for 20 h, respectively. The residual concentration of metal ion was also measured using ICP-AES. To further investigate the adsorption mechanism, adsorption thermodynamics studies were also carried out as: 10 mg UiO-66-TA was added into 20 mL gold solution (initial concentration 200 ppm) and shaken for 20 h under different temperature (25 °C, 35 °C and 45 °C).

The removal rate and adsorption capacity were calculated as Eqs. (1) and (2):

$$R_0 = \frac{(C_0 - C_r)}{C_0} \times 100\% \quad (1)$$

$$q_e = \frac{(C_0 - C_r)}{W} \times V \quad (2)$$

where R_0 (%) was the removal rate of Au(III); C_0 and C_r (ppm) were represented the initial concentration and equilibrium concentration of Au(III); q_e (mg/g) was the adsorption capacity; and V and W were solution volume (mL) and adsorbent dosage (mg) respectively.

3. Results and discussion

3.1. Characterization

As shown in Fig. 1, the synthesis of the adsorbent was characterized by FTIR. It can be seen in the spectrum of UiO-66-NH₂ that the main

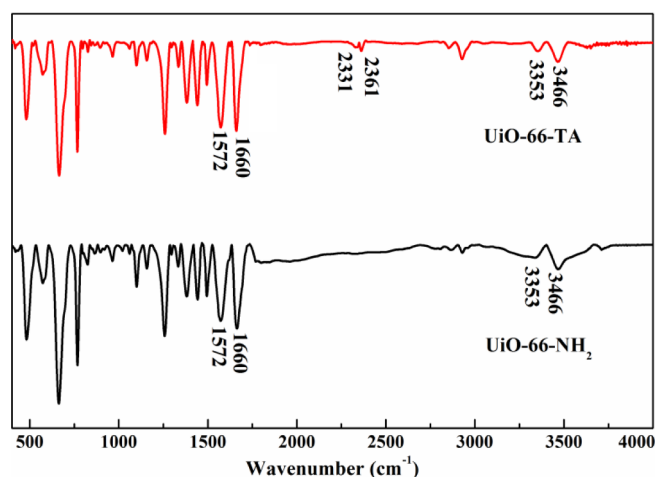


Fig. 1. FTIR spectrum of UiO-66-types.

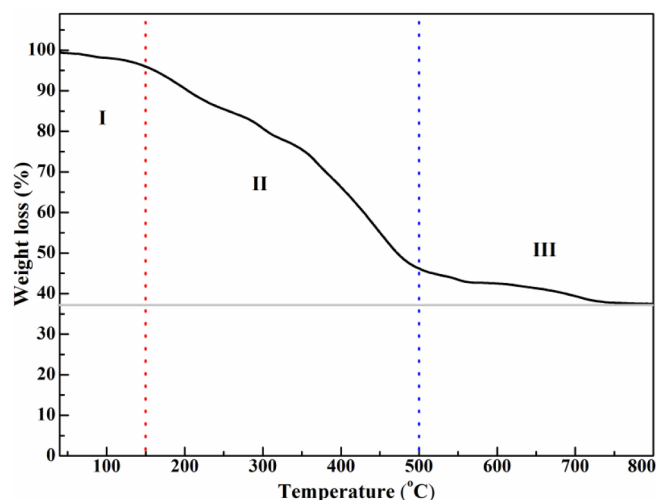


Fig. 2. The thermogravimetric analyze of UiO-66-TA.

peaks appeared at 1572 cm⁻¹, 1660 cm⁻¹, 3353 cm⁻¹ and 3466 cm⁻¹. 1572 cm⁻¹ and 1660 cm⁻¹ represented the synergy of carboxyl and Zr⁴⁺. 3353 cm⁻¹ and 3466 cm⁻¹ represented N–H bond [22]. After modification with thioctic acid, some new peaks appeared in the spectrum of UiO-66-TA. The peak at 1736 cm⁻¹ corresponded to C=O bond and the peak at 2331 cm⁻¹ and 2361 cm⁻¹ corresponded to S–S bond. Those new peaks proved that the synthesis of UiO-66-TA was successful.

The thermogravimetric analyze of UiO-66-TA was shown in Fig. 2. The weight loss of UiO-66-TA with temperature was divided into two steps. In step I (room temperature to 150 °C), the weight loss was just 10% and attributed to the adsorbed water. In step II (150 °C–500 °C), the weight loss reached to 54% and the main reason was the combustion of organic matter. In this part, the structure was destroyed. In the last step, the weight loss is negligible with increasing temperature, which is due to the fact that the crystals of UiO-66-TA were destroyed and only organic Zr was left in the combustion of organic matter. In summary, UiO-66-TA can maintain excellent thermal stability below 150 °C.

The specific surface area and pore size are important factors affecting the adsorption capacity. Therefore, UiO-66-NH₂ and UiO-66-TA were characterized by BET. The related data was presented in Table 1. With the modification of thioctic acid, the surface area dropped from 702.2 m²/g to 505 m²/g and total pore volume dropped from 4.1 nm to 2.6 nm, indicating that UiO-66-TA still maintains a superior pore structure and has been successfully modified.

The surface morphology of UiO-66-NH₂ and UiO-66-TA were presented in Fig. 3 via FESEM. Obviously, both UiO-66-NH₂ and UiO-66-TA were nanomaterials and octahedral shapes. In addition, the TEM spectra was consistent with the microscopic morphology in the literature [23]. They had little differences in size and shapes, indicating that the addition of thioctic acid does not destroy the structure of Zr-MOF.

3.2. Effect of pH

Solution pH was studied to expose the possible interaction

Table 1
Surface area of UiO-66-NH₂ and UiO-66-TA.

Category	UiO-66-NH ₂	UiO-66-TA
Surface area (m ² /g)	702.2	505
Average pore size (nm)	1.17	0.96
Total pore volume (cm ³ /g)	4.1	2.6

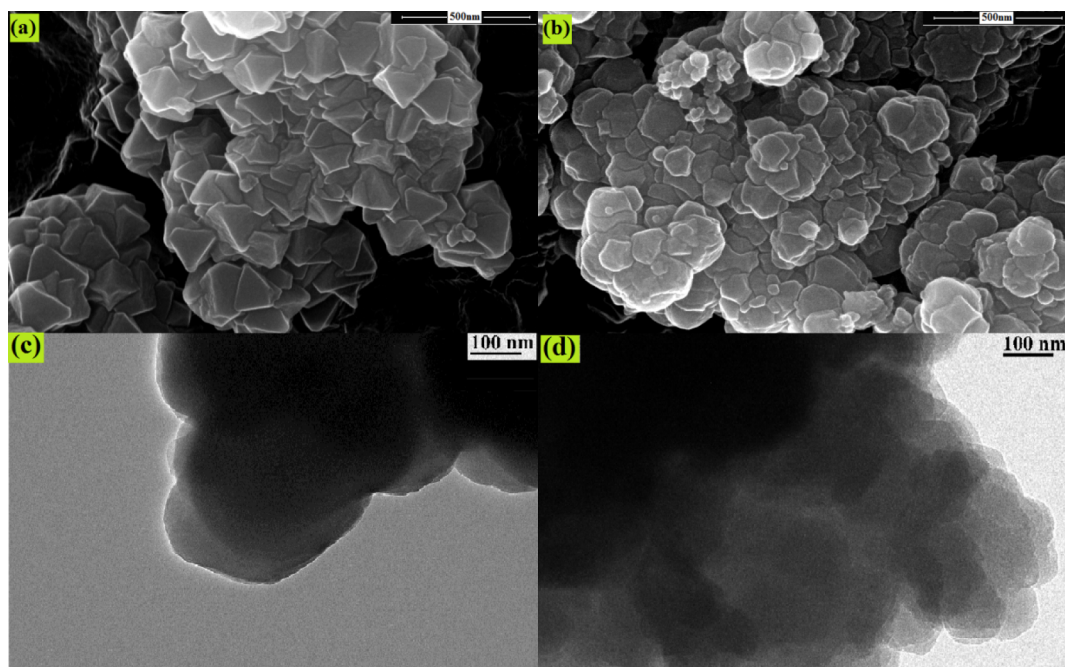


Fig. 3. The SEM spectra (a and b) and the TEM spectra (c and d) of UiO-66-NH₂ and UiO-66-TA.

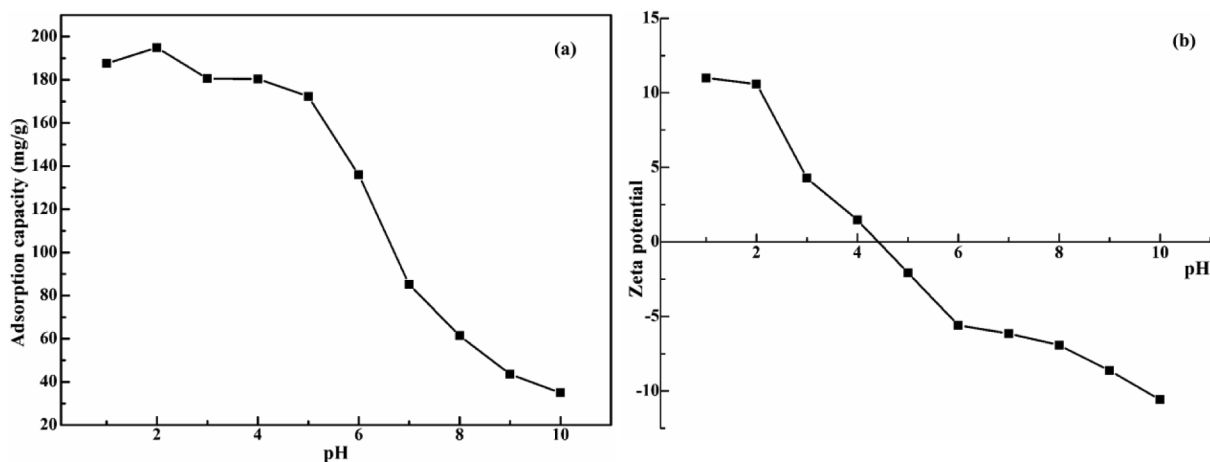


Fig. 4. The adsorption capacity (a) and the zeta potential (b) of UiO-66-TA.

mechanism of UiO-66-TA with Au(III). As shown in Fig. 4(a), the adsorption capacity of UiO-66-TA increased with the increasing of pH from 1 to 2 and decreased with the decreasing of pH from 2 to 10. The zeta potentials of UiO-66-TA and Au (III) solution were also presented in Fig. 4(b). Obviously, the zeta potential was decreased with the decreasing of pH. Moreover, the isoelectric point of UiO-66-TA was pH 4.4, indicating that the zeta potential was positive below pH 4.4 and negative over pH 4.4. With pH below 4.4, the sulfur-containing groups on the surface of UiO-66-TA were protonated, enhancing the binding of the sulfur-containing groups to Au(III). With pH increased over 4.4, the concentration of OH⁻ has increased, competing with the adsorption site on the surface of UiO-66-TA. In summary, ion exchange is one of the main adsorption mechanism between UiO-66-TA and Au(III).

3.3. Adsorption kinetic

In order to explore the effect of reaction time on adsorption of UiO-66-TA for Au(III), adsorption kinetic was conducted to explore the mechanism. The adsorption capacity of UiO-66-TA for Au(III) was

shown in Fig. 5(a). Obviously, the fastest adsorption occurred in the first 30 min, reaching at 162 mg/g. During this period, the UiO-66-TA surface has enough adsorption sites that can be combined with Au(III) ions. As the adsorption sites are occupied in large quantities, the speed of adsorption was slowed down and the balanced adsorption capacity reached within 240 min.

The adsorption behaviors were affected by many factors, such as diffusion control, chemical reaction and interparticle diffusion. For exploring the adsorption behavior, three kinetic models were adopted, including PFO, PSO and interparticle diffusion model. They can be expressed by the following three equation (Eqs. (3)–(5)), respectively [24,25]:

$$\ln(q_e - q_t) = \ln q_e - k_1 t \quad (3)$$

$$\frac{t}{q_t} = \frac{1}{k_2 q_e^2} + \frac{t}{q_e} \quad (4)$$

$$q_t = k_3 t^{1/2} + C \quad (5)$$

where k_1 , k_2 and k_3 are the rate constant of pseudo-first-order (PFO),

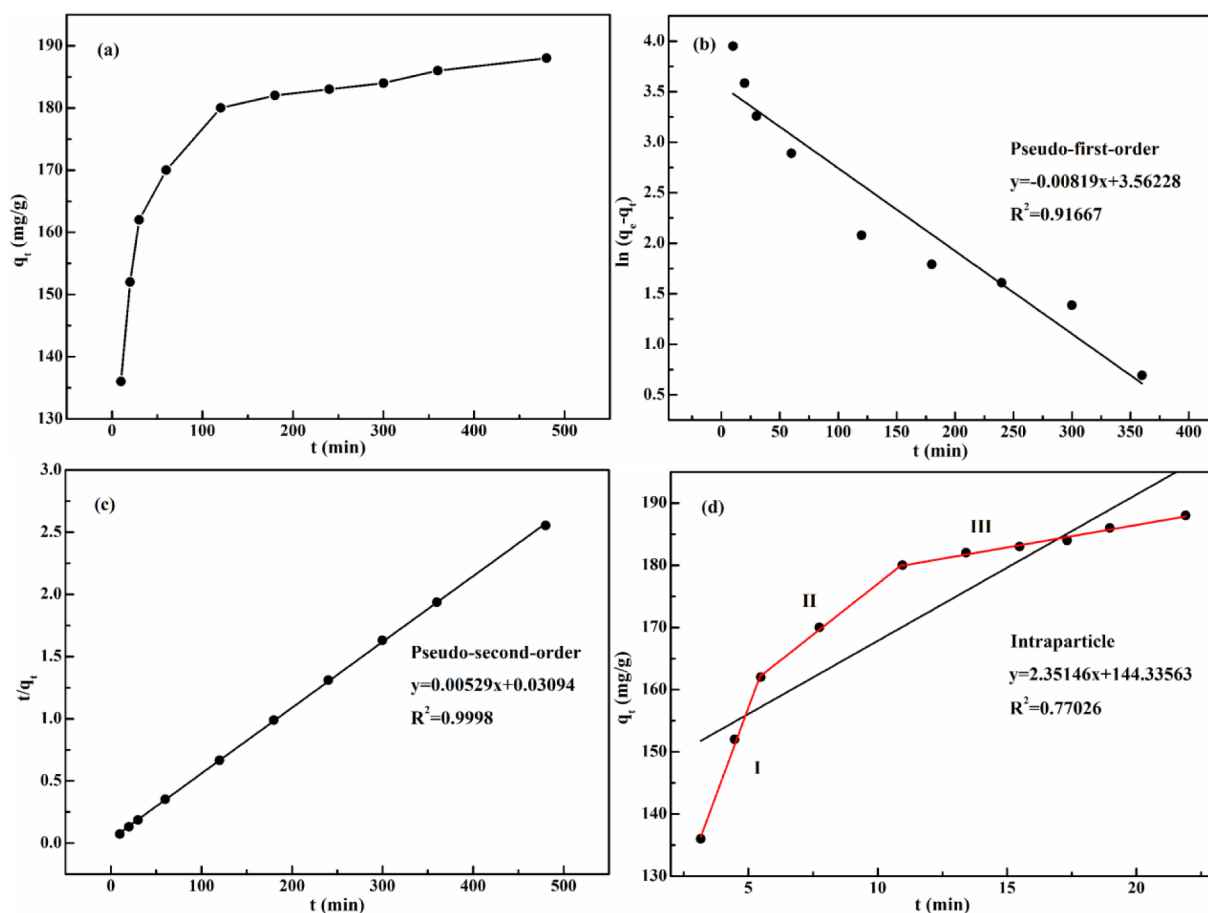


Fig. 5. (a) Effect of reaction time on gold sorption, linear isotherm models for Au(III) adsorption on UiO-66-TA (b) PFO, (c) PSO and (d) intraparticle.

pseudo-second-order (PSO) and interparticle diffusion model, respectively. q_t is the adsorption capacity at time t . C is a constant of interparticle diffusion model.

The PFO model describes that the surface of adsorbent decides the speed of adsorption and the PSO model describes that the chemical reaction decides the speed of adsorption. The fitting straight line and the related parameters were presented in Fig. 5(b and c) and Table 2. Obviously, the R^2 value of PSO model (0.9998) was far greater than PFO model (0.91667). In addition, Δq value of PSO model was smaller than PFO model. The fitting of PSO model of Au(III) on UiO-66-TA was better than that of PFO model, indicating that the chemical reaction was the main adsorption behavior.

For further research, interparticle diffusion model was also adopted to explore the adsorption behavior. After the fitting straight line, the related parameters were shown in Fig. 5(d) and Table 3. Obviously, it can be divided into three parts and the R^2 values were 0.639, 0.997 and 0.984, respectively. The gold ions rapidly diffuse to the surface of UiO-66-TA at the first stage while gold ions begin to penetrate from the surface of the adsorbent to the inside at the second stage. In the last

Table 2

The parameters of the PFO and PSO kinetic models.

Kinetic models	Parameters	Values
PFO	q_e	35.243
	k_1	-0.008
	R^2	0.917
PSO	q_e	189.036
	k_2	0.005
	R^2	0.99998

Table 3

The parameters of three parts in intraparticle diffusion model.

Parameters	Part I	Part II	Part III
C	100.701	144.272	172.02
k_3	11.28	3.275	0.723
R^2	0.639	0.9976	0.98429

part, the adsorption has reached saturation and has little changes. The adsorption behavior in the intraparticle diffusion of UiO-66-TA was complex linear process.

3.4. Adsorption isotherm

To further explore the adsorption capacity of modified UiO-66-TA, the adsorption isotherms were conducted with different Au(III) initial concentration for UiO-66-NH₂ and UiO-66-TA, respectively. The relationships between Au(III) initial concentration and adsorption capacity were shown in Fig. 6(a). The adsorption capacity increased with the increasing of Au(III) initial concentration. The adsorption capacity of UiO-66-NH₂ and UiO-66-TA reached saturation (158 mg/g and 372 mg/g) when the initial concentration goes to 900 mg/L, indicating that the modification improves the maximum adsorption capacity of the adsorbent.

In order to better explore the mechanism of isotherm adsorption, three isotherm models were used for analysis. Langmuir isotherm model (L) mainly verifies whether the adsorption mechanism is a single layer adsorption of a uniform surface. Freundlich isotherm (F) model primarily verifies that adsorption occurs on uneven surfaces. Temkin isotherm (T) model mainly verifies whether the heat of adsorption

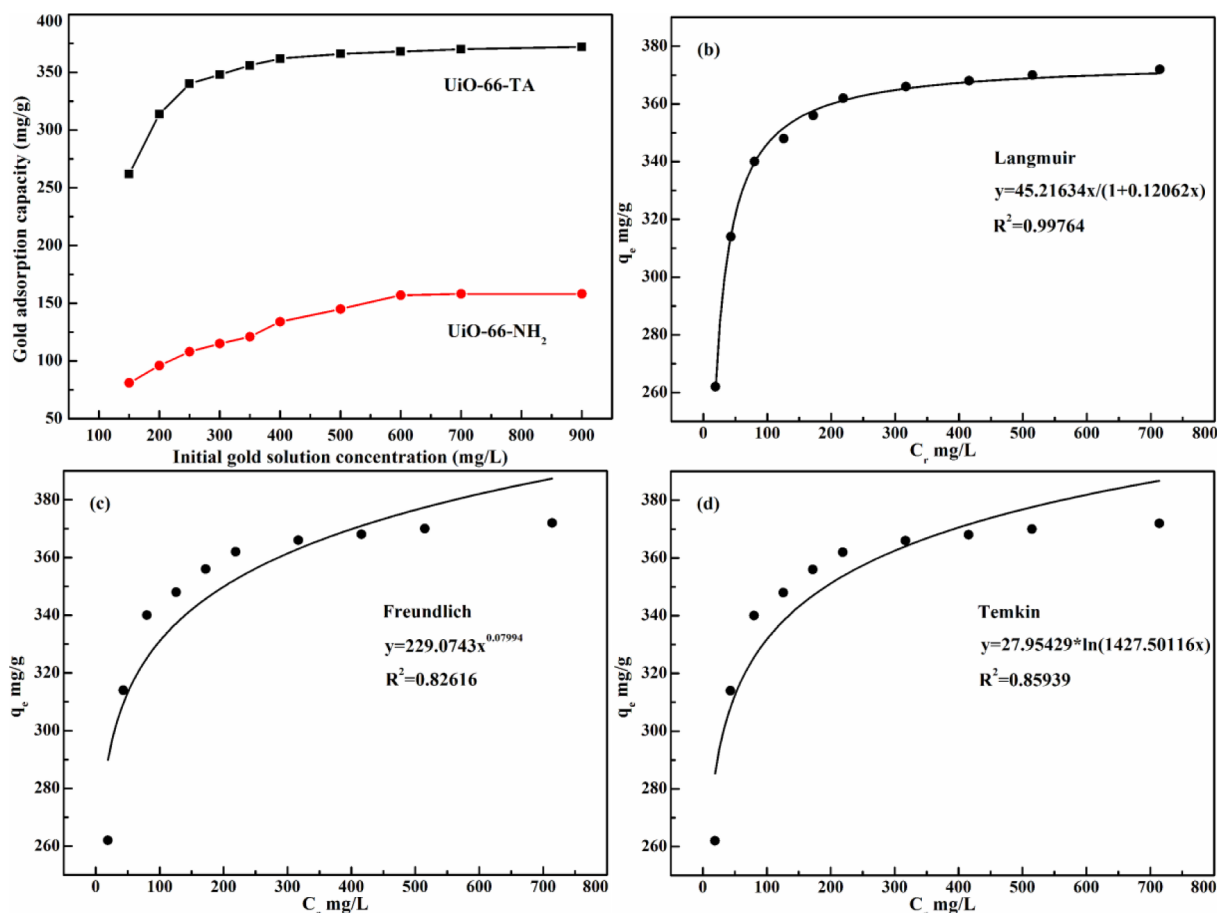


Fig. 6. (a) Effect of initial Au(III) concentration on sorption of UiO-66-NH₂ and UiO-66-TA for gold, nonlinear isotherm models for Au(III) adsorption on UiO-66-TA (b) Freundlich, (c) Langmuir and (d) Temin.

decreases as the adsorbent and adsorbate interact in different adsorbent layers. L, F and T isotherm models can be expressed by Eqs. (6)–(8) [26–28]:

$$q_e = \frac{k_L q_m C_r}{1 + k_L C_e} \quad (6)$$

$$q_e = K_F C_r^{1/n} \quad (7)$$

$$q_e = \frac{RT \ln(K_T C_r)}{\beta} \quad (8)$$

where K_L , K_F and K_T represent the constants of L, F and T isotherm models, respectively. q_e is the equilibrium adsorption capacity and C_e is the residual concentration of Au(III) ion solution. In addition, the $1/n$ value represents the adsorption capacity index. β is a constant while R

and T are the constant of universal gas, temperature in Kelvin, respectively.

The fitting curve and the related parameters were presented in Fig. 6(b–d) and Table 4. F model had a R^2 value of 0.826 and the adsorption capacity index $1/n$ showed a value (0.07994) between 0 and 1, indicating that the adsorption was advantageous. T model had a R^2 value of 0.859 and the heat of adsorption indicated that a strong interaction exist between the reactive group and the Au(III) ion. Nevertheless, the R^2 value of L model (0.997) was larger than that of F and T model. Moreover, the theoretical maximum adsorption capacity (374.866 mg/g) is very close to the actual maximum adsorption amount (372 mg/g) and the error is less than 1%, indicating that the L model can be better described isotherm adsorption.

High adsorption capacity is an important advantage of UiO-66-TA. Various adsorbents in the literature were placed in Table 5 for comparison. Obviously, UiO-66-TA has a higher adsorption capacity than the other adsorbents.

3.5. Regeneration experiments

In order to reduce costs and protect the environment, the reusability of the adsorbent is very important. Therefore, regeneration experiments were conducted to explore the reusability of UiO-66-TA. 30 mg UiO-66-TA was added to 60 mL Au(III) solutions and shaken for 24 h. The gold ion concentration in supernatant was measured after centrifugation. During the desorption experiment, 80 mL 10% thiourea solution (2% HCl) was added to the centrifuge tube containing the precipitate and shaken for 24 h. After that, the regenerated adsorbent is washed with deionized water for 5 times. As shown in Fig. 7, the whole experiment

Table 4

The fitting parameters of isotherm models.

Model	Parameter	Value
Langmuir	q_m (mg/g)	374.866
	K_L (L/g)	0.121
	R^2	0.99764
Freundlich	K_F (mg g ⁻¹ (L mg ⁻¹) ^{1/n})	229.074
	$1/n$	0.08
	R^2	0.82616
Temkin	β	81.198
	K_T (L/g)	1427.501
	R^2	0.85939

Table 5
Comparison of Various adsorbents in the literature for gold adsorption.

Adsorbents	Functional group	q_{\max} (mg/g)	pH	Kinetics (min)	Literature
Polymer	1,8-Diaminonaphtalene-formaldehyde/PVC	62.3	1.0	6000	[29]
Chitosan	Glisin	169.98	2.0	100	[30]
Silica	diethylenetriaminemethylenephosphonic acid	357.14	2.0	60	[31]
montmorillonite	alginate	1.49	3.0	93.00	[32]
Nanosilica	guanidinium ionic liquid	120.56	5.0	150	[33]
oil palm trunk	–	91	4.1	360	[34]
lignocellulosic	Aminopropyltriethoxysil-ane	261.36	4.0	120	[35]
Raw date pits	–	78	1.0	120	[36]
Resin	glutamicum biomass	361.7	3.0	1440	[37]
Zr-MOF	thioctic acid	372	2	240	This work

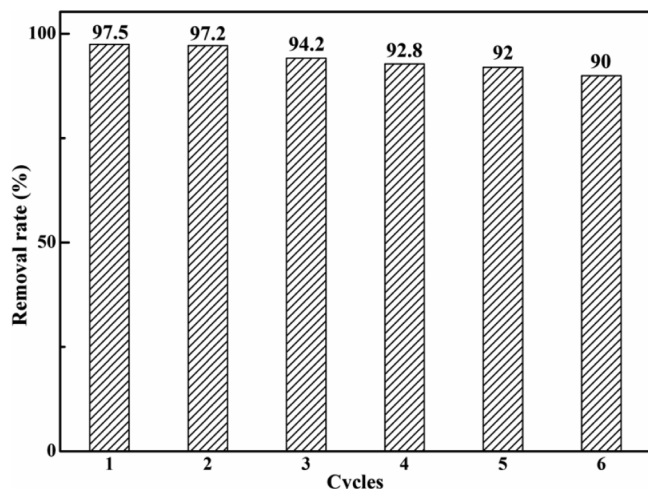


Fig. 7. Reusability of UiO-66-TA.

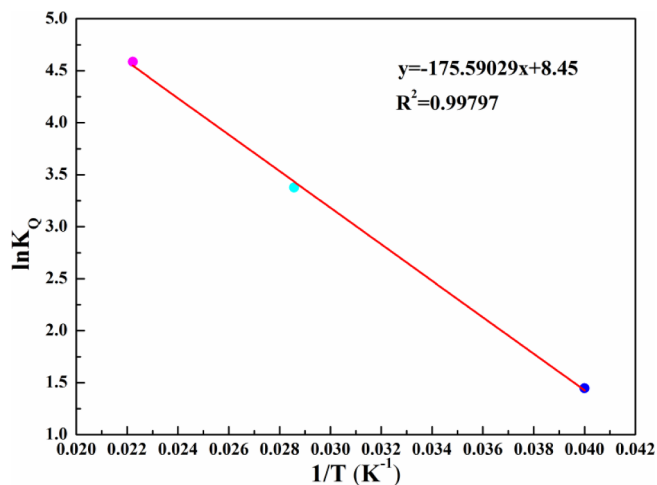


Fig. 8. Effect of temperature on Au(III) adsorption.

Table 6
Related parameters of Thermodynamic experiment.

ΔH_{θ} ($J mol^{-1} K^{-1}$)	ΔS_{θ} ($J mol^{-1}$)	T (K)	ΔG_{θ} ($J mol^{-1}$)	R^2
1459.85767	70.2533	298	-19475.6257	0.99797
		308	-20178.1587	
		318	-20880.6917	

was conducted for 6 times and the adsorption capacity decreased from 97.5% to 90%. Obviously, UiO-66-TA still maintains a high adsorption capacity for gold ions after multiple regenerations.

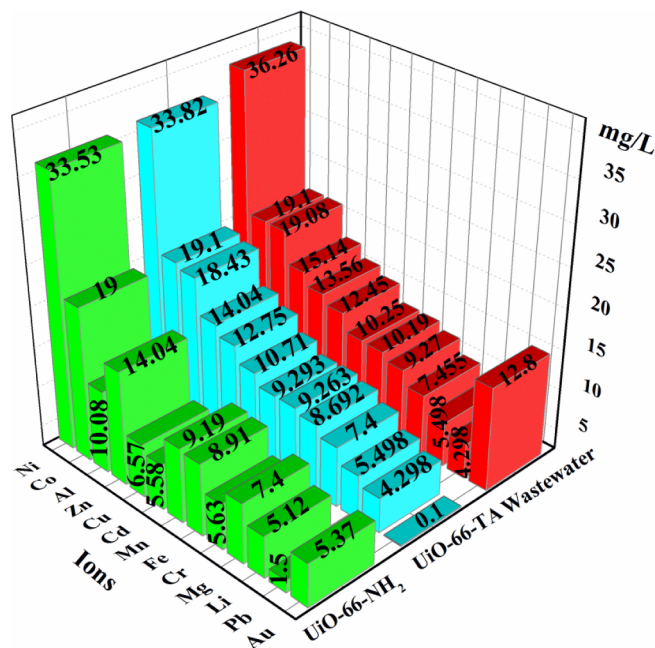


Fig. 9. Effect of Au(III) adsorption in wastewater.

Table 7
 K_Q and K of the mixed ions in wastewater.

Metal ions	K_Q (mL/g)	K
Au(III)	239,600	–
Pb(II)	0	$+\infty$
Li(II)	0	$+\infty$
Mg(II)	14.86	16123.82
Cr(II)	133	1801.5
Fe(III)	1854	129.23
Mn(II)	1914	125.18
Cd(II)	324.93	737.39
Cu(II)	127.06	1885.72
Zn(II)	156.7	1529.04
Al(III)	70.54	3396.65
Co(II)	0	$+\infty$
Ni(II)	144.29	1660.54

3.6. Thermodynamic experiment

In order to explore the relationship between adsorption capacity and temperature, thermodynamic experiment was conducted. The research was conducted under conditions of 298 K, 308 K and 318 K. The related parameters are calculated with Eqs. (9) and (10) [38], including Entropy change (ΔS_{θ}), transmutation (ΔH_{θ}) and Gibbs free energy (ΔG_{θ}).

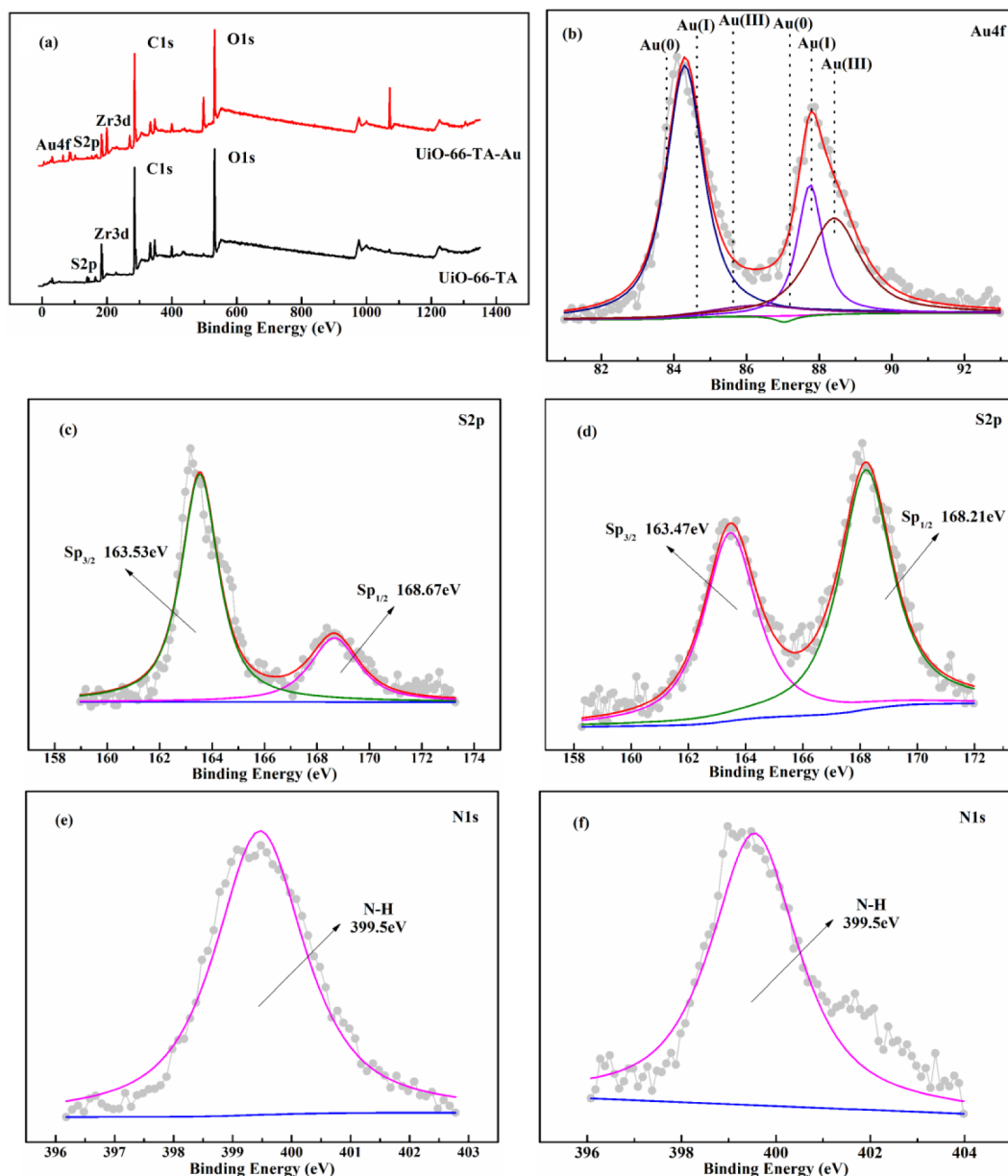


Fig. 10. XPS spectra of UiO-66-TA (a) and Au4f of UiO-66-TA-Au (b), S2p of UiO-66-TA (c) and UiO-66-TA-Au (d), N1s of UiO-66-TA (e) and UiO-66-TA-Au (f).

$$\ln K_s = \frac{-\Delta G_\theta}{RT} = \frac{\Delta S_\theta}{R} - \frac{\Delta H_\theta}{RT} \quad (9)$$

$$\Delta G_\theta = \Delta H_\theta - T\Delta S_\theta \quad (10)$$

where $R(8.314 \text{ J mol}^{-1} \text{ K}^{-1})$ and T are gas constant and experiment temperature (Kelvin), respectively. K_s was the distribution coefficient.

As shown in Fig. 8, $\frac{1}{T}$ and $\ln K_s$ expressed the relationship between sorption capacity and temperature, which obtained from the experiment. The related parameters were shown in Table 6, the value of ΔH_θ and ΔS_θ were positive, indicating that the entire process is an endothermic process. The value of ΔG_θ was negative, indicating that the adsorption is spontaneous.

3.7. Wastewater application

In order to verify the difference between UiO-66-NH₂ and UiO-66-TA in practice, adsorption experiments were carried out in laboratory wastewater. After the pH adjustment, the metal ions contained in the wastewater were measured, including Au, Pb, Li, Mg, Cr, Fe, Mn, Cd,

Cu, Zn, Al, Co and Ni. The relative relationships were shown in Fig. 9. Obviously, UiO-66-NH₂ adsorbed limited gold ions and maintains high adsorption capacity for various impurity ions. However, UiO-66-TA still maintains a high adsorption capacity for gold ions from multi-ion wastewater and the impurity ions in the wastewater are not adsorbed, indicating that UiO-66-TA has better selectivity than UiO-66-NH₂. In order to explore the selectivity of UiO-66-TA, the distribution coefficient (K_Q) and selectivity coefficient (K) were adopted. The ions can be well adsorbed with the large K_Q value while the ions still distributed in solution with the small K_Q value. K_Q and K can be expressed by Eqs. (11) and (12) [39]:

$$K_Q = \frac{Q}{C_e} = \frac{C_i - C_e}{C_e} \cdot \frac{V}{m} \quad (11)$$

$$K = \frac{K_{Q(\text{Au}^{3+})}}{K_{Q(\text{coexisting ions})}} \quad (12)$$

As shown in Table 7, The K_Q value of Au(III) was larger than that of the other ions, indicating that the interaction between Au(III) and UiO-

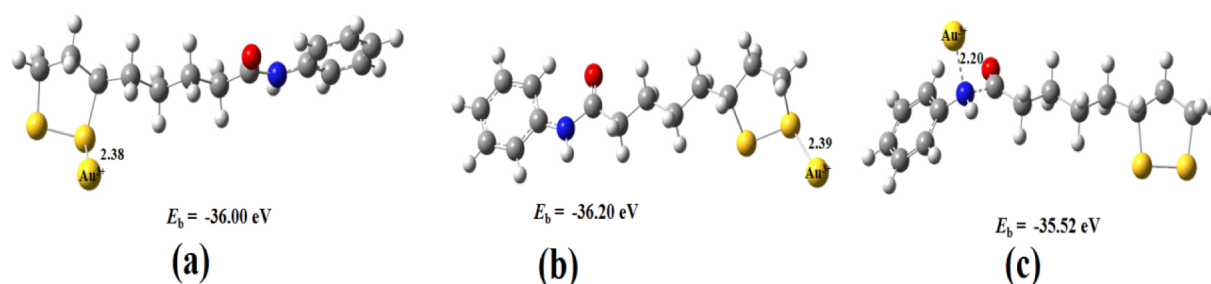


Fig. 11. The optimized geometries of the complexes and the binding energy, as well as the bond length. (a) Au^{3+} on O; (b, c) Au^{3+} on S; (d) Au^{3+} on N. The grey, white, red, blue, yellow and yellow with Au^{3+} corresponds to C, H, O, N, S and Au atoms, respectively. (For interpretation of the references to colour in this figure legend, the reader is referred to the web version of this article.)

66-TA was the strongest. Moreover, the large k values of UiO-66-TA for mixed ions suggested that the functional group has a low affinity for interfering ions. In summary, UiO-66-TA has a good prospect with long-term consideration.

3.8. Adsorption mechanism

3.8.1. XPS analysis

For exploring the adsorption mechanism, XPS of UiO-66-TA and UiO-66-TA-Au were investigated. As shown in Fig. 10(a), the spectrum of Au4f appeared after adsorption and could be divided into three chemical state, including Au(III), Au(I) and Au(0). The peak of Au(III) appeared at 86.3 eV ($\text{Au}4f_{7/2}$) and 88.41 eV ($\text{Au}4f_{5/2}$). The peak of Au(I) appeared at 84.3 eV ($\text{Au}4f_{7/2}$) and 87.75 eV ($\text{Au}4f_{5/2}$). The peak of Au(0) appeared at 83.34 eV ($\text{Au}4f_{7/2}$) and 87.04 eV ($\text{Au}4f_{5/2}$). The reduction reaction of gold is shown in Eqs. (13) and (14):



As shown in Fig. 10(c), the spectrum of S2p consisted of two peaks, including 163.53 eV and 168.67 eV. They were $\text{Sp}_{3/2}$ and $\text{Sp}_{1/2}$, indicating that the modification of Zr-MOF with thioctic acid was successful. The spectrum of S2p after adsorption was presented in Fig. 10(d) and the two peaks were shifted from 163.53 eV and 168.67 eV to 163.47 eV and 168.21 eV, respectively. The shift in the peak of S2p was mainly due to the chelation of the sulfur-containing functional group with the gold ion. In addition, it can be seen from Fig. 10(e and f) that the XPS peak of N–H does not change after adsorption.

3.8.2. DFT calculation

In practice, DFT calculations provide accurate information about the energy of adsorption through theoretical calculations to better understand the nature of the interaction during the adsorption [40]. DFT calculations can be used to better analyze interactions in the adsorption process. In this part, all the structures, energies, and frequencies were calculated at the B3LYP level (Becke's three-parameter nonlocal-exchange functional with the nonlocal correlational of Lee et al. method) based on GAUSSIAN 09 program [27,28]. For the basis set, the LANL2DZ basis set was employed for Au and the 6–31 + G(d,p) basis sets were used for other atoms. According to experimental results, in this work Au^{3+} is used as the model of $\text{Au}(\text{Cl})_4^-$. To investigate the stability of the complexes, the binding energy (E_b) is evaluated by Eq. (15) [41,42]:

$$E_b = E_{\text{total}} - E_{\text{Au}^{3+}} - E_{\text{sub}} \quad (15)$$

where, E_{total} is the total energy of complexes, $E_{\text{Au}^{3+}}$ and E_{sub} are the isolated Au^{3+} and substrate, respectively. A negative value indicates a stable chemisorption.

The optimized geometries of the complexes and the important

geometry parameters are illustrated in Fig. 11. The binding energies of Au–N and Au–S bonds are negative, indicating the Au^{3+} intends to coordinate with the nitrogen and sulfur atoms of UiO-66-TA through monodentate coordination. However, the binding energy of gold and sulfur is significantly stronger than the binding energy of gold and nitrogen. So, the main adsorption method is the combination of gold and sulfur because the more negative the binding energy, the stronger the interaction between the metal-adsorbent complexes. DFT calculation results are highly consistent with the order of binding affinity observed from the experimental results, which proves the summative selective adsorption mechanism.

4. Conclusion

In this work, a new adsorbent (UiO-66-TA) was successfully prepared by modifying UiO-66- NH_2 with thioctic acid. Its adsorption properties were evaluated by integrated experimental measurement with adsorption system modeling. With excellent specific surface area and a special shape, adsorption of Au(III) ions with UiO-66-TA appeared to be quickly (240 min) and the adsorption capacity of UiO-66-TA (372 mg/g) is obviously improved relative to UiO-66- NH_2 (158 mg/g). Experiment models manifested that the process was the chemical adsorption on a uniform surface. The adsorption capacity improved with the enhancing of temperature, indicating that it was a spontaneous endothermic process. UiO-66-TA achieved high selectivity than UiO-66- NH_2 in wastewater. In addition, UiO-66-TA can be reused at least six times. With the XPS analysis and DFT calculation, it can be found that the adsorption of gold ions relies on the synergy of functional groups on UiO-66-TA and the sulfur-containing functional groups play a major role therein. In summary, UiO-66-TA can be an excellent adsorbent in the future wastewater treatment.

Acknowledgement

This work was supported by the National Natural Science Foundation of China (U1702252).

References

- [1] X. Huang, Y. Wang, X. Liao, B. Shi, Adsorptive recovery of Au^{3+} from aqueous solutions using bayberry tannin-immobilized mesoporous silica, *J. Hazard. Mater.* 183 (2010) 793–798.
- [2] G. Lin, S. Wang, L. Zhang, T. Hu, J. Peng, S. Cheng, L. Fu, C. Srinivasakannan, Selective recovery of Au(III) from aqueous solutions using 2-aminothiazole functionalized corn bract as low-cost bioadsorbent, *J. Cleaner Prod.* 196 (2018) 1007–1015.
- [3] S. Lin, K.R.D. Harikishore, J.K. Bediako, M.H. Song, W. Wei, J.A. Kim, Y.S. Yun, Effective adsorption of Pd(II), Pt(IV) and Au(III) by Zr(IV)-based metal-organic frameworks from strongly acidic solutions, *J. Mater. Chem. A* 5 (2017) 13557–13564.
- [4] S. Rascón-Leon, M.M. Castillo-Ortega, I. Santos-Sauceda, G.T. Munive, D.E. Rodríguez-Félix, T. Del Castillo-Castro, J.C. Encinas, J.L. Valenzuela-García, J.M. Quiroz-Castillo, B. García-Gaitan, P.J. Herrera-Franco, J. Alvarez-Sanchez, J.Z. Ramírez, L.S. Quiroz-Castillo, Selective adsorption of gold and silver in bromine

- solutions by acetate cellulose composite membranes coated with polyaniline or polypyrrole, *Polym. Bull.* 75 (2018) 3241–3265.
- [15] R. Khosravi, A. Azizi, R. Ghaedrahmati, V.K. Gupta, S. Agarwal, Adsorption of gold from cyanide leaching solution onto activated carbon originating from coconut shell—optimization, kinetics and equilibrium studies, *J. Ind. Eng. Chem.* 54 (2017) 464–471.
- [16] H. Murakami, S. Nishihama, K. Yoshizuka, Separation and recovery of gold from waste LED using ion exchange method, *Hydrometallurgy* 157 (2015) 194–198.
- [17] G. Li, Z. Zhao, J. Liu, G. Jiang, Effective heavy metal removal from aqueous systems by thiol functionalized magnetic mesoporous silica, *J. Hazard. Mater.* 192 (2011) 277–283.
- [18] K.F. Lam, K.L. Yeung, G. McKay, An investigation of gold adsorption from a binary mixture with selective mesoporous silica adsorbents, *J. Phys. Chem. B* 110 (2006) 2187.
- [19] S. Kim, S. Park, S. Han, Y. Han, J. Park, Silanol-rich ordered mesoporous silica modified thiol group for enhanced recovery performance of Au(III) in acidic leachate solution, *Chem. Eng. J.* 351 (2018) 1027–1037.
- [20] G. Lin, T. Hu, S. Wang, T. Xie, L. Zhang, S. Cheng, L. Fu, C. Xiong, Selective removal behavior and mechanism of trace Hg(II) using modified corn husk leaves, *Chemosphere* 225 (2019) 65–72.
- [21] G.-P. Li, K. Zhang, P.-F. Zhang, W.-N. Liu, W.-Q. Tong, L. Hou, Y.-Y. Wang, Thiol-functionalized pores via post-synthesis modification in a metal-organic framework with selective removal of Hg(II) in water, *Inorg. Chem.* 58 (2019) 3409–3415.
- [22] N.D. Rudd, H. Wang, E.M.A. Fuentes-Fernandez, S.J. Teat, F. Chen, G. Hall, Y.J. Chabal, J. Li, Highly efficient luminescent metal-organic framework for the simultaneous detection and removal of heavy metals from water, *ACS Appl. Mater. Interfaces* 8 (2016) 30294–30303.
- [23] L. Ding, X. Luo, P. Shao, J. Yang, D. Sun, Thiol-functionalized Zr-based metal-organic framework for capture of Hg(II) through a proton exchange reaction, *ACS Sustain. Chem. Eng.* 6 (2018) 8494–8502.
- [24] W. Ke, J. Gu, Y. Na, Efficient removal of Pb (II) and Cd (II) using NH₂-functionalized Zr-MOFs via rapid microwave-promoted synthesis, *Ind. Eng. Chem. Res.* 56 (2017).
- [25] S.-W. Lv, J.-M. Liu, H. Ma, Z.-H. Wang, C.-Y. Li, N. Zhao, S. Wang, Simultaneous adsorption of methyl orange and methylene blue from aqueous solution using amino functionalized Zr-based MOFs, *Microporous Mesoporous Mater.* 282 (2019) 179–187.
- [26] S.N. Tambat, P.K. Sane, S. Suresh, N.O. Varadan, A.B. Pandit, S.M. Sontakke, Hydrothermal synthesis of NH₂-UiO-66 and its application for adsorptive removal of dye, *Adv. Powder Technol.* 29 (2018) 2626–2632.
- [27] A.M. Ploskonka, J.B. DeCoste, Tailoring the adsorption and reaction chemistry of the metal-organic frameworks UiO-66, UiO-66-NH₂, and HKUST-1 via the incorporation of molecular guests, *ACS Appl. Mater. Interfaces* 9 (2017) acsami.7b06274.
- [28] Z.-W. Chang, Y.-J. Lee, D.-J. Lee, Adsorption of hydrogen arsenate and dihydrogen arsenate ions from neutral water by UiO-66-NH₂, *J. Environ. Manage.* 247 (2019) 263–268.
- [29] K.-Y.A. Lin, Y.-T. Liu, S.-Y. Chen, Adsorption of fluoride to UiO-66-NH₂ in water: stability, kinetic, isotherm and thermodynamic studies, *J. Colloid Interface Sci.* 461 (2016) 79–87.
- [30] L. Fu, S. Wang, G. Lin, L. Zhang, Q. Liu, J. Fang, C. Wei, G. Liu, Post-functionalization of UiO-66-NH₂ by 2,5-Dimercapto-1,3,4-thiadiazole for the high efficient removal of Hg(II) in water, *J. Hazard. Mater.* 368 (2019) 42–51.
- [31] B. Fotoohi, L. Mercier, Some insights into the chemistry of gold adsorption by thiol and amine functionalized mesoporous silica in simulated thiosulfate system, *Hydrometallurgy* 156 (2015) 28–39.
- [32] L. Fu, S. Wang, G. Lin, L. Zhang, Q. Liu, H. Zhou, C. Kang, S. Wan, H. Li, S. Wen, Post-modification of UiO-66-NH₂ by resorcylic aldehyde for selective removal of Pb (II) in aqueous media, *J. Cleaner Prod.* 229 (2019) 470–479.
- [33] W.G. Tian, C. Xiao, R.V. Maligal-Ganesh, X. Li, W. Huang, Utilizing mixed-linker zirconium based metal-organic frameworks to enhance the visible light photocatalytic oxidation of alcohol, *Chem. Eng. Sci.* 124 (2015) 45–51.
- [34] Y.-d. Huang, Comments on using of “pseudo-first-order model” [Appl. Surf. Sci. 394 (2017) 378–385, 397 (2017) 133–143, 426 (2017) 545–553, 437 (2018) 294–303], *Appl. Surf. Sci.* 469 (2019) 564–565.
- [35] H. Moussout, H. Ahlafi, M. Aazza, H. Maghat, Critical of linear and nonlinear equations of pseudo-first order and pseudo-second order kinetic models, *Karbala Int. J. Mod. Sci.* 4 (2018) 244–254.
- [36] J. Couble, D. Bianchi, Experimental microkinetic approach of the CO/H₂ reaction on Pt/Al₂O₃ using the Temkin formalism. 2. Coverages of the adsorbed CO and hydrogen species during the reaction and rate of the CH₄ production, *J. Catal.* 352 (2017) 686–698.
- [37] I. Langmuir, The adsorption of gases on plane surfaces of glass, mica and platinum, *J. Am. Chem. Soc.* 40 (1918) 1361–1403.
- [38] H. Freundlich, Over the adsorption in solution, *J. Phys. Chem.* 57 (1906) 1100–1107.
- [39] Ü.C. Erim, M. Gülfen, A.O. Aydın, Separation of gold(III) ions by 1,8-diaminonaphthalene-formaldehyde chelating polymer, *Hydrometallurgy* 134–135 (2013) 87–95.
- [40] A. Ramesh, H. Hasegawa, W. Sugimoto, T. Maki, K. Ueda, Adsorption of gold(III), platinum(IV) and palladium(II) onto glycine modified crosslinked chitosan resin, *Bioresour. Technol.* 99 (2008) 3801–3809.
- [41] W. Liu, P. Yin, X. Liu, X. Dong, J. Zhang, Q. Xu, Thermodynamics, kinetics, and isotherms studies for gold(III) adsorption using silica functionalized by diethylenetriaminemethylenephosphonic acid, *Chem. Eng. Res. Des.* 91 (2013) 2748–2758.
- [42] A. Mourpichai, T. Jintakosol, W. Nitayaphat, Adsorption of gold ion from a solution using montmorillonite/alginate composite, *Mater. Today: Proc.* 5 (2018) 14786–14792.
- [43] C. Xiong, Y. Li, S. Wang, Y. Zhou, Functionalization of nanosilica via guanidinium ionic liquid for the recovery of gold ions from aqueous solutions, *J. Mol. Liq.* 256 (2018) 183–190.
- [44] N. Saman, J.-W. Tan, S.S. Mohtar, H. Kong, J.W.P. Lye, K. Johari, H. Hassan, H. Mat, Selective biosorption of aurum(III) from aqueous solution using oil palm trunk (OPT) biosorbents: equilibrium, kinetic and mechanism analyses, *Biochem. Eng. J.* 136 (2018) 78–87.
- [45] N. Saman, M.U. Rashid, J.W.P. Lye, H. Mat, Recovery of Au(III) from an aqueous solution by aminopropyltriethoxysilane-functionalized lignocellulosic based adsorbents, *React. Funct. Polym.* 123 (2018) 106–114.
- [46] H.M. Al-Saidi, The fast recovery of gold(III) ions from aqueous solutions using raw date pits: kinetic, thermodynamic and equilibrium studies, *J. Saudi Chem. Soc.* 20 (2016) 615–624.
- [47] I.S. Kwak, M.A. Bae, S.W. Won, J. Mao, K. Sneha, J. Park, M. Sathishkumar, Y.-S. Yun, Sequential process of sorption and incineration for recovery of gold from cyanide solutions: comparison of ion exchange resin, activated carbon and biosorbent, *Chem. Eng. J.* 165 (2010) 440–446.
- [48] E.C. Lima, A. Hosseini-Bandegharaei, J.C. Moreno-Piraján, I. Anastopoulos, A critical review of the estimation of the thermodynamic parameters on adsorption equilibria. Wrong use of equilibrium constant in the Van't Hoff equation for calculation of thermodynamic parameters of adsorption, *J. Mol. Liq.* 273 (2019) 425–434.
- [49] Y. Tian, P. Yin, R. Qu, C. Wang, H. Zheng, Z. Yu, Removal of transition metal ions from aqueous solutions by adsorption using a novel hybrid material silica gel chemically modified by triethylenetetraminomethylenephosphonic acid, *Chem. Eng. J.* 162 (2010) 573–579.
- [50] I. Matrane, M. Mazroui, Y. Boughaleb, Diffusion and adsorption of Au and Pt adatoms on ideal and missing row reconstructed surfaces of Au(110): DFT and EAM calculations, *Surf. Sci.* 677 (2018) 83–89.
- [51] H. Farrokhpour, M. Ghandehari, K. Eskandari, ONIOM DFT study of the adsorption of cytosine on the Au/Ag and Ag/Au bimetallic nanosurfaces: the effect of sublayer, *Appl. Surf. Sci.* 457 (2018) 712–725.
- [52] S. Ahmad, R. Ahmad, M. Bilal, N.U. Rehman, DFT studies of thermoelectric properties of R-Au intermetallics at 300 K, *J. Rare Earths* 36 (2018) 197–202.